ASME Journal of Engineering and Science in Medical Diagnostics and Therapy
Online journal at:
https://asmedigitalcollection.asme.org/medicaldiagnostics

Eve Sobirey[1]
Institute of Product Development and Mechanical Engineering Design, Hamburg University of Technology, Denickestr. 17, Hamburg 21073, Germany
e-mail: eve.sobirey@tuhh.de

Jonte Schmiech
Institute of Product Development and Mechanical Engineering Design, Hamburg University of Technology, Denickestr. 17, Hamburg 21073, Germany
e-mail: jonte.schmiech@tuhh.de

Marie Wegner
Institute of Product Development and Mechanical Engineering Design, Hamburg University of Technology, Denickestr. 17, Hamburg 21073, Germany
e-mail: marie.wegner@tuhh.de

Fabian Flottmann
Department of Diagnostic and Interventional Neuroradiology, University Medical Center Hamburg-Eppendorf, Martinistraße 52, Hamburg 20251, Germany
e-mail: f.flottmann@uke.de

Matthias Bechstein
Department of Diagnostic and Interventional Neuroradiology, University Medical Center Hamburg-Eppendorf, Martinistraße 52, Hamburg 20251, Germany
e-mail: m.bechstein@uke.de

Maximilian Jungnitz
Department of Diagnostic and Interventional Neuroradiology, University Medical Center Hamburg-Eppendorf, Martinistraße 52, Hamburg 20251, Germany
e-mail: m.jungnitz@uke.de

Martin Oertel
Department of Diagnostic and Interventional Neuroradiology, University Medical Center Hamburg-Eppendorf, Martinistraße 52, Hamburg 20251, Germany
e-mail: m.oertel@uke.de

Middle Meningeal Artery Model for Training Endovascular Treatment of Chronic Subdural Hematomas in Interventional Neuroradiology

Technical progress and the development of smaller treatment instruments allow neurointerventional procedures to be used to treat diseases involving small vessels (< 2 mm). One example is the subdural hematoma (SDH), which can be treated by embolizing the middle meningeal artery (MMA) to cut off blood supply to SDH. The procedure was first used in 2018, following efficacy and safety studies. The embolization is technically very challenging and requires extensive training of the physicians. This work presents the development of an MMA model for endovascular training simulations of SDH with original instruments and particle embolization for integration into the existing neurointerventional training simulator Hamburg ANatomical NEurointerventional Simulator (HANNES). The development and testing were carried out by an interdisciplinary team of physicians and engineers. The aim of this work is to avoid the disadvantages of animal experiments, such as ethical aspects, anatomical differences to human vessel architecture, and long-term availability. First, a printing study of the MMA model was carried out to determine suitable processes and materials. Subsequently, suitable models were tested by experienced neurointerventional physicians in a realistic treatment setting, whereby they assessed 4 out of 20 models as sufficiently good. Relevant criteria were, among others, the flowrate, probing ability, elasticity, haptics, and geometric mapping. Based on these findings, an embolization module was developed to capture particles during training, which was evaluated as a moderate basic model for SDH embolization training. In conclusion, the novel MMA model with embolization module integrated in the simulator HANNES enables an innovative state-of-the-art neurointerventional training opportunity of physicians. [DOI: 10.1115/1.4068146]

Keywords: interventional neuroradiology, endovascular therapy, chronical subdural hematoma, cSDH, embolization, particle embolic agent, ContourTM, simulation model, HANNES, 3D printing

[1]Corresponding author.
Contributed by the Applied Mechanics Division Technical Committee on Dynamics & Control of Structures & Systems (AMD-DCSS) of ASME for publication in the Journal of Engineering and Science in Medical Diagnostics and Therapy. Manuscript received October 2, 2024; final manuscript received January 8, 2025; published online March 28, 2025. Editor: Ahmed Al-Jumaily.

Jens Fiehler
Department of Diagnostic and
Interventional Neuroradiology,
University Medical Center Hamburg-Eppendorf,
Martinistraße 52,
Hamburg 20251, Germany
e-mail: fiehler@uke.de

Dieter Krause
Institute of Product Development and
Mechanical Engineering Design,
Hamburg University of Technology,
Denickestr. 17,
Hamburg 21073, Germany
e-mail: krause@tuhh.de

Introduction

Over the past few decades, medicine has made significant progress in the areas of diagnosis, treatment, and therapy. In particular, in the field of neuroradiology, the development of neurointerventional procedures has revolutionized the understanding and treatment of neurological diseases. During neurointerventional procedures, the pathological vessels are localized and treated via a catheter, which is advanced into the target vessel under X-ray control. This method, which is also known as endovascular treatment (EVT), has increasingly become the standard treatment in the field of cerebral vascular medicine over the last few years, reducing the need for open surgery [1,2]. Cerebrovascular diseases affect the blood vessels in the brain, including narrowing, occlusion, or vessel wall rupture causing strokes or cerebral hemorrhage [3]. With the technological progress in the development of treatment instruments and neurovascular materials, it is now possible to use neurointerventional procedures to treat diseases involving small peripheral vessels [4,5]. Navigating the treatment instruments inside these small vessels as well as locating the diseased artery poses specific challenges. In cerebral vascular medicine, this comprises in particular the procedures for treating small vessels with a diameter of under 2 mm, including the middle meningeal artery (MMA), which plays a key role in the development of chronic subdural hematomas (cSDH). A cSDH is a hemorrhage in the subdural space, a space between the hard and soft meninges [6]. The cSDH is an encapsulated collection of fluid, blood, and blood degradation products, which is typically found as a half-moon-shaped formation along the cerebral hemisphere on a computer tomography (CT) image (see Fig. 1(*a*)) [6]. The traditional method used to treat cSDH is open surgery with burr hole trepanation or craniotomy [7]. This involves opening the skull to remove the hematoma and aspirate the blood [5,8,9]. This procedure has a recurrence rate of up to 37% due to an inflammatory reaction caused by the residual blood [10]. The blood supply to the membranes surrounding and feeding the hematoma is provided by the MMA [10], which is closed with an embolic agent in a neurointerventional procedure [5,8]. This MMA embolization (MMAE) procedure is less invasive and has a significantly lower recurrence rate [8]. A contrast agent induced digital subtraction angiography (DSA) image of the MMA and the characteristic curve of the artery passing the foramen spinosum is shown in Fig. 1(*b*).

Endovascular treatment of cerebral vascular disease is a rapidly evolving field that covers a variety of neurointerventional instruments. This requires physicians to have not only anatomic and clinical knowledge but also the understanding of the appropriate selection and use of instruments and catheters. As EVT of cSDH with particle embolic agents is a relatively new treatment concept, there is a need for systematic training of interventional physicians and further practice. For training purposes, animal models are mostly used despite disadvantages, including ethical aspects as well as the unrealistic anatomical replication of the human brain [11,12].

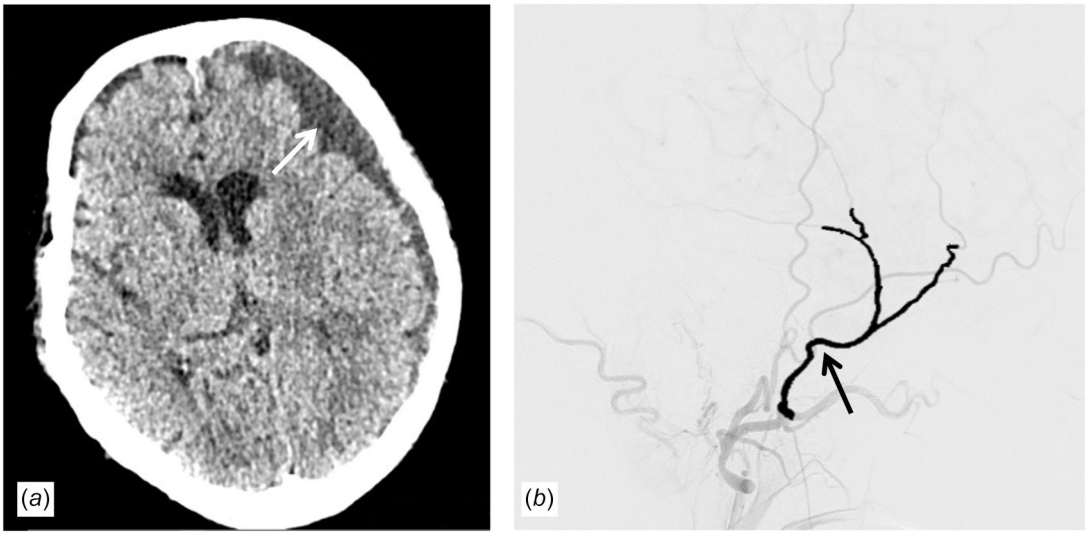

Fig. 1 (*a*) Computer tomography image of a SDH highlighted by a black arrow and (*b*) DSA image of the MMA highlighted by a black arrow

In addition, as animal experiments are difficult to reproduce because it is necessary to artificially generate the subdural hematoma (SDH) by implanting clotted blood into the subdural space [13]. To improve this situation, the development of a model for integration into a physical simulator is required, allowing training simulations of SDH with original instruments, particle embolic agents, and patient-based geometry.

Current Models for Endovascular Treatment Training of Subdural Hematoma Using Embolization

An analysis of the existing cSDH training methods shows that the research into MMAE treatment, education, and training still appears to be in its beginnings. In the literature, many studies of clinical outcomes of patients with MMAE or comparison studies of open surgery and MMAE can be found [14–22]. In addition, studies have been carried out on various embolization techniques and embolic agents like particle embolic agents, liquid embolic agents, and coil embolization [23–28]. Particle embolic agents are the most commonly used embolic agents due to their long-term efficacy and proven safety [21,26,27]. This paper is therefore focused on this embolization procedure. The studies on MMAE have provided important findings on the effectiveness and clinical outcomes of these interventions, but largely leave unconsidered aspects of education and training in MMAE. The focus in the training of neuroradiologists is on animal-based models [29], while MMAE training is represented weakly with only two animal model experiments in swine [11,12]. These animal models have significant negative aspects such as long-term availability, anatomical replication of human structures, ethical issues, and the artificial creation of disease in animals to simulate realistic training conditions. Prognostic models [30,31] and finite element methods (FEM) [32–34] are increasingly being developed and used to better understand the disease progression and recovery process. These simulations offer valuable insights, particularly in predicting therapy outcomes. Furthermore, deep learning (DL) models are being developed and used for the detection of SDH [35–37]. However, a physical simulation model that specifically enables the treatment of cSDH using MMAE by particle embolization with original instruments in a real angiography suite is currently lacking. Such a model could bridge the gap from training to treatment and significantly improve training and further education in this relatively new form of therapy.

Development of the Middle Meningeal Artery Model With Embolization Module

The MMA model for endovascular training treatment of cSDH was developed through close collaboration between an interdisciplinary team of physicians and engineers. By combining medical expertise and technical knowledge, the model was designed to replicate realistic anatomy and reproduce the complexity and particularities of the neurointerventional procedure as accurately as possible. The development of the training simulation model for cSDH treatment was carried out in two phases. First, an MMA model was developed and the suitability of different manufacturing processes and materials was investigated. Then, an embolization module was designed and manufactured.

The developed model was integrated into an overall training setup. The simulator HANNES (Hamburg ANatomical NEurointerventional Simulator), which is already utilized for training applications under real conditions in angiography for aneurysm, stroke, and stenosis treatment, is used for this purpose [38–41]. HANNES has a vascular tree from the femoral artery to the cerebral vessels to simulate the entire endovascular procedure of cerebral vascular diseases. The different patient-based additively manufactured vascular models enable an edge-free connection using standardized connectors and can be easily exchanged due to their modular structure [38,40]. A realistic blood pressure is simulated by a fluid system with individually adjustable temperature, pulse, and volume flow individually. The fluid used is water with baby shampoo, as described by Schmiech et al. [41].

Requirements and Design of the Middle Meningeal Artery Model. The development of the MMA model was based on the VDI 2221 guidelines [42] (Development of technical products and systems—Model of product development) with the steps planning, conception, design and development, and the standardized process flow of Spallek et al. [38], for the development of vessel models from image data acquisition to design, manufacturing and application. First, the requirements for the MMA model to be developed were analyzed in an interview with the physicians and documented in the form of a requirements list. According to Wegner et al., the requirements can be classified in the aspects of geometrical, physiological, and medical therapy mapping [43]. The MMA model should replicate a patient-based geometry with anatomically correct diameters to simulate the difficulty of treating small vessels diseases. In addition, the anatomical landmark of the foramen spinosum, which is a strong curve specific to the course of the MMA in the body, should be replicated in the model (see Fig. 1(*b*) black arrow).

Similarly, to the existing vascular models integrated in HANNES, the MMA model should also have a hollow inner structure as well as a smooth surface and no edges. Regarding material-specific requirements, the model should not be manufactured using metallic materials to avoid imaging artifacts. Furthermore, the material of the MMA model should be liquid-tight and water-resistant. The model developed is to be integrated into the HANNES training model for simulation of the entire treatment process with original treatment devices.

The standardized process flow of Spallek et al. [13] with the steps of medical data acquisition, the design of specifications and the production of the model up to the application was applied to develop and produce the MMA model. Figure 2 shows the different process steps from segmentation to design and additive manufacturing. First, the physicians three-dimensional (3D)-rotational angiography is used to acquire image data of the MMA from an anonymous patient. This high-resolution image data served as the basis for further processing. Using the Seg3D segmentation software (NIH Center for Integrative Biomedical Computing at the University of Utah), the relevant vessels of the patient were precisely segmented by the physicians. The first step was to generate a threshold-based preselection, which was then manually postprocessed. This step is important as it ensures that only the essential vascular structures are selected and extracted for the model. The resulting segmented model of the MMA was converted into a Standard Triangulation Language file (STL) to prepare the data for further processing. The STL file is a common format in 3D printing and computer-aided design (CAD), as it describes the geometric information in the form of triangular surfaces. In the next step, the segmented image data was used to design a detailed and hollow MMA vessel model in the CAD program CATIA (Dassault Systèmes, Vélizy Villacoublay, France). The model was analyzed in CATIA to determine the inner diameters using the "wall thickness anaylsis" tool with the sphere method. Figure 3 shows the internal volume of the hollow model with diameters, $d > 2$ mm (blue), $2 \leq d \leq 0.8$ mm (green), and $d < 0.8$ mm (red). The model was subsequently provided with a wall thickness of 1 mm on the outside and enhanced with standardized interfaces. For this purpose, the existing edge-free connector was used to integrate the model into the vessel tree of the HANNES simulator (see in Fig. 4). Additionally, four outlet hose connectors were integrated (see in Fig. 4). The wall thickness was developed iteratively for existing larger brain vessel models for HANNES and applied to the MMA models to find a compromise between mechanical stability and a material-saving design.

The final designed MMA model with all connectors was prepared for manufacturing by creating another STL file.

Manufacturing of the Middle Meningeal Artery Model. The MMA models were fabricated from various materials using different additive manufacturing processes to investigate what might be suitable for the manufacturing of small vessel models. The different additive manufacturing processes such as stereolithography (SLA),

Fig. 2 Process steps for the development and manufacturing of the MMA model from segmentation to design and additive manufacturing based on the standardized process flow from Spallek et al. [38]

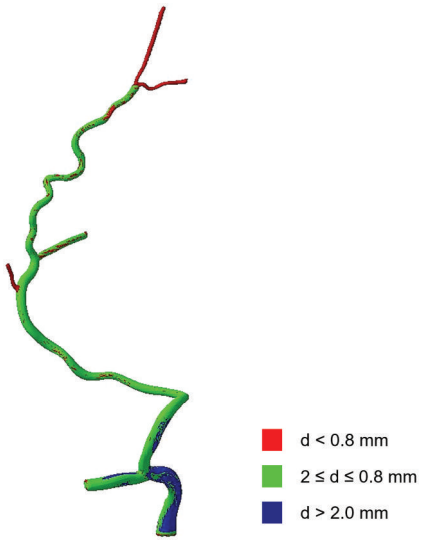

Fig. 3 Analysis of the inner diameters of the internal volume of the hollow MMA model using the sphere method in CATIA with diameters, $d > 2$ mm (blue), $2 \leq d \leq 0.8$ mm (green), and $d < 0.8$ mm (red)

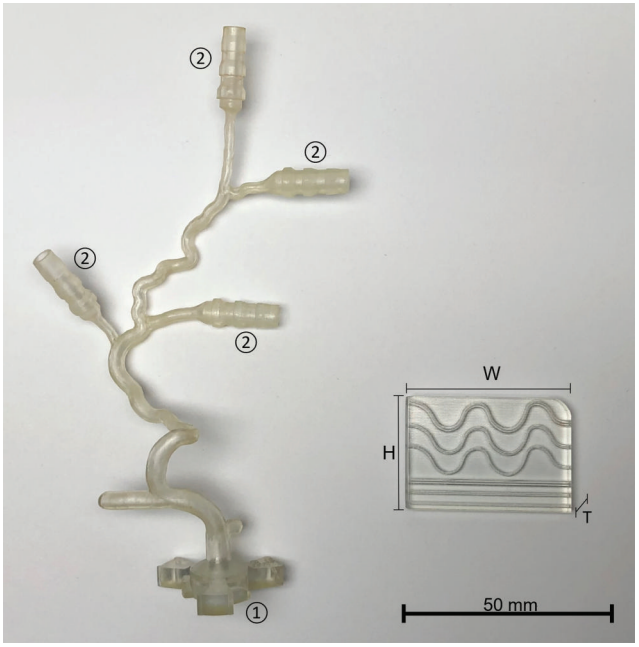

Fig. 4 SLA-manufactured models made of watershed material: (*a*) MMA model with edge-free connector and hose connectors and (*b*) block model with height (H), width (W) and thickness (T) with straight and curved channels with diameters of 1.5 mm, 1 mm, and 0.8 mm

fused deposition modeling (FDM), and polyjet technology (PJ) were analyzed. Either an external manufacturer was consulted or the models were produced in-house. Production of the MMA model using selective laser sintering (SLS) was rejected by various manufacturers due to the difficulty of residue-free removal of the support structures or the impossibility of fabricating small hollow structures. A total of ten SLA models (SLA1-10), two FDM models (FDM1-2) and eight polyjet models (PJ1-8) were analyzed. The materials vary from elastic to hard and transparent to nontransparent. Due to the different elastic properties, the relevance of the elasticity of the models for replicating realistically is to be investigated in a blind test by the physicians. Transparent MMA models theoretically have the potential for X-ray-free evaluation, enabling training without X-rays or additional analysis. A summary of the investigated processes and materials as well as their technical specifications the hardness of the materials are listed in Table 1. As a reference, a block with small channels was designed and printed in order to investigate whether the production of complex MMA models is difficult but simpler components could be manufactured using the respective additive manufacturing process and material. The block has the dimensions 40 mm (W) × 28 mm × (H) 5 mm (T) and contains six channels, three linear and three curved. The diameters of the channels are 1.5 mm, 1 mm, and 0.8 mm respectively and are arranged in descending order from top to bottom of the component. Figure 4 shows an example of the block and the MMA model produced using the SLA process made of watershed material.

Requirements and Conceptual Design of the Embolization Module. The development of the embolization module is also based on VDI2221, and the requirements were again defined in cooperation with the physicians first. Similarly, to the MMA model,

Table 1 Summary of the manufacturing specifications and properties of the models from different additive manufacturing processes and materials. The layer thickness and resolution specifications are based on manufacturer information.

Model ID	Material	3D Printer	Layer thickness (μm)	Resolution (μm)	Hardness	Transparency
FDM1*	PETG	Anycubic i3 Mega	200	12.5	80-90D	No
FDM2*	ABS	Ultimaker S5	150	6.9 × 6.9	n/a	No
PJ1	Agilus 70	Stratasys J750	27	27	70A	No
PJ2	Agilus 30	Stratasys J750	27	27	30A	No
PJ3	Vero clear	Stratasys J750	27	27	80-84D	Yes
PJ4	High-detail resin	n/a	n/a	n/a	83D	No
PJ5	Vulcan soft elastomer	Inkbit Vista	28	32 × 63.5 × 18	30A	No
PJ6	AR-G1H	Agilista 3200 W	30	63.5 × 40	65A	Yes
PJ7	AR-G1 L	Agilista 3200 W	30	63.5 × 40	35A	Yes
PJ8*	AR-G1 L	Agilista 3200 W	30	63.5 × 40	35A	Yes
SLA1	Accura ClearVue	3D Systems - SLA 5000	100	n/a	84D	Yes
SLA2	WaterShed® XC 11122	3D Systems - SLA Viper	100	n/a	85D	Yes
SLA3	Standard resin	n/a	n/a	n/a	n/a	Yes
SLA4	Transparent resin	n/a	n/a	n/a	81D	Yes
SLA5	Accura Xtreme	Prox800 von 3D Systems	100	n/a	86D	No
SLA6*	Flexible 80A	Form 3	50	25	80A	Yes
SLA7*	Elastic 50A V1	Form 3	100	25	50A	Yes
SLA8*	Clear V4	Form 3	25	25	82D	Yes
SLA9*	63A	Photon M3	50	40	63A	Yes
SLA10*	82A	Photon M3	50	40	82A	Yes

Note: The models marked with * are in-house fabrication.

the embolization module should also have a hollow inner structure as well as a smooth surface and no edges. Furthermore, the real embolization behavior in the model and the realistic embolization distribution under X-ray imaging are important requirements. The training of the treatment with embolization should result in a partial to complete flow disruption, as in humans. Furthermore, the reusability of the model after embolization is desired. Like the MMA model, the module should not be made of metallic materials, taking into account the material-specific requirements to avoid artifacts in imaging. The developed module should be integrated into the HANNES training model to simulate the entire treatment process with an edge free connection to the MMA model.

Once the requirements have been established, the conceptual design phase begins as described in VDI2221 [42]. This involves developing a functional structure that maps the main and subfunctions necessary of the embolization module. This structure is used to identify different working principles for each subfunction and supports a systematic approach to the design process. Figure 5 shows the hierarchical function structure developed for the embolization module. In this structure, the primary goal of "enable embolization treatment training for SDH in HANNES" is divided into several subfunctions, such as "enable embolization treatment with original instruments" and "implement module in HANNES." Each of these subfunctions is further subdivided into more specific tasks, such as "visualize embolization" and "avoid complete blockage during embolization." The morphological box was chosen as the methodology for working out partial solutions to the subfunctions developed in the hierarchical function structure. This methodology is intended to help analyze complex problems and find many different approaches to solutions. Several alternative solutions were developed based on this, which were then evaluated using a weighted scoring system according to technical criteria such as anatomically correct mapping of embolization and economic criteria such as production costs. The best-rated alternative solution was then selected and developed.

Design and Manufacturing of the Embolization Module. The solution for the embolization module was a corpus with an integrated membrane. It was designed in a CAD program (Autodesk Inventor, San Rafael, United States) and modified with connectors for integration into the MMA model in the simulator HANNES. The additively manufactured embolization module with the components corpus and the membrane size of 25 mm as well as the connector for integration with the MMA model and the hose connector can be seen in Fig. 6. The corpus was manufactured from the material Clear V4 (Formlabs Inc., Somerville, MA) in two different sizes using the SLA printers Form 3 (Formlabs Inc.) available in-house for different membrane sizes. The membranes used were borosilicate glass membranes (Reichelt Chemietechnik GmbH, Heidelberg, Germany) in diameters of 10 mm and 25 mm with different pore sizes of 40 μm and 160 μm. The small pore sizes are aimed at stopping the flow of particle embolic agents.

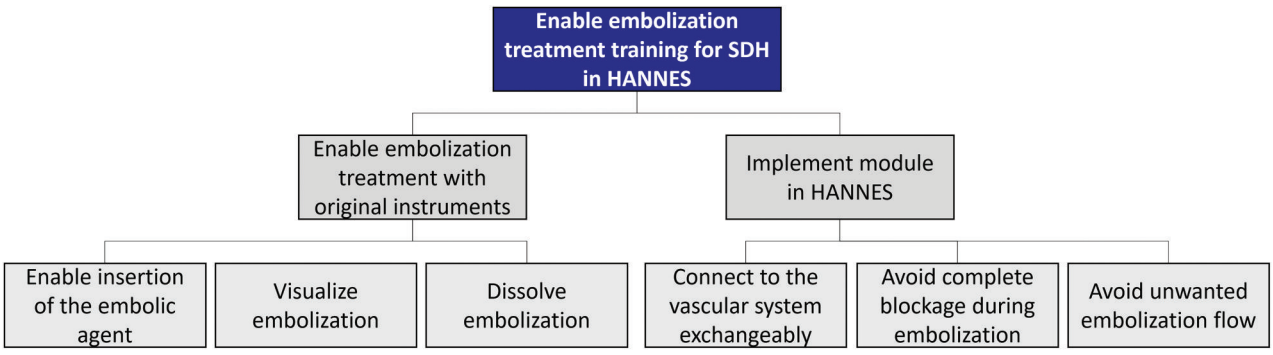

Fig. 5 Hierarchical functional structure developed for the embolization module, illustrating the key functions and subfunctions necessary for a treatment simulation of SDH in HANNES

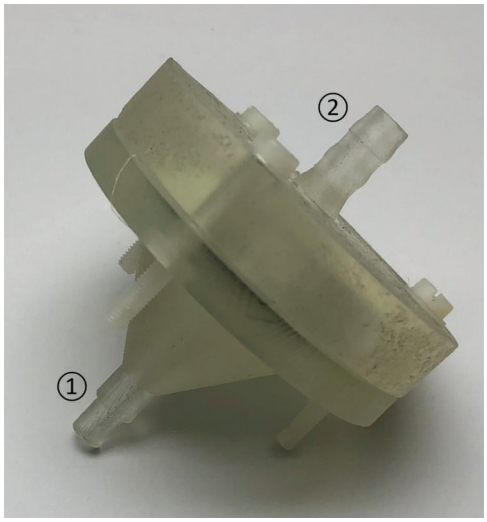

Fig. 6 Additively manufactured embolization module made up of a corpus and a borosilicate glass membrane with a diameter of 25 mm and the connector for integration with the MMA model and the hose connector

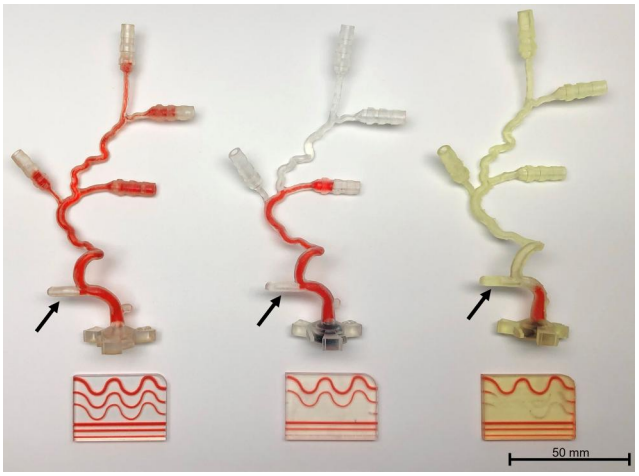

Fig. 7 Colored cavities of the MMA models and blocks made of the materials SLA1 (left), SLA8 (middle) and SLA10 (right). The black arrow marks the occluded, not flowed-through outlet of the maxillary artery.

Results

The comparison of the different manufactured MMA models and the application of the embolization module focus on the real use by neuroradiologists with original treatment instruments and the Contour^{TM} particle embolic agent (Boston Scientific, Marlborough, MA) used with different particle sizes from 45 μm to 150 μm and 150 μm to 250 μm polyvinyl alcohol particle size in the simulation model HANNES. The results are divided into the MMA models with their properties and the application tests. For the embolization module, the results are presented in two stages. First, the outcome of the pretests on the behavior of the embolic agent outside the body in a water circuit is first described. Following this, the results of the tests conducted by the physicians are explained.

Middle Meningeal Artery Model Preliminary Investigation. The comparison of the differently manufactured MMA models focuses on their properties with regard to their suitability for training catheter-based interventions. First, the entire cavity of the MMA model has to be accessible and open. The vascular models must be liquid-tight in order to be used in angiography with water and contrast medium. In addition, the materials should not swell during long-term use in the simulation model with water. Furthermore, the roughness of the materials has to allow easy navigation of the catheter.

Manufacturing. The in-house production of the FDM models presented a challenge. The cavities of the MMA models could not be printed freely and the models broke during manufacturing or while removing the support structures. The breakage could be avoided by increasing the wall thickness of the MMA model or using more elastic materials than the FDM1 and FDM 2. In general, FDM printers offer lower resolution and detail accuracy compared to SLA or PJ printers, especially when used for printing small, fine structures and smooth surfaces. In the following, the properties of the FDM-printed models are analyzed, but no application tests are carried out.

Vessel Cavities and Liquid Tightness. To examine the cavities and liquid tightness, water with red food coloring was injected into the MMA models as well as into the blocks of transparent materials to identify the continuity of the models. Water was also injected into the nontransparent models to check if water was flowing out of any outlets. In order to avoid an occlusion in the simulation model, only continuous MMA models with at least one free outlet can be analyzed for their suitability of the training simulation. Figure 7 shows the colored cavities of the MMA models and blocks made of the materials SLA1 (left), SLA8 (middle) and SLA10 (right). The SLA1 models has free cavities throughout the MMA model and the block, while the MMA model made of SLA10 is almost completely sealed. However, the block demonstrates that printing of small straight channels and some curved channels is possible. The models made of SLA8 show a moderately good result, as some free cavities can be recognized. The summary of all results from the vessel cavities 20 MMA models can be seen in Fig. 8. All FDM models have closed vessel cavities and are not liquid-tight, leading to water leaks out of the walls of the blocks. Three of the PJ models have no open vessels, while four models have completely open vessels. All three closed models were produced on the same 3D printer (Stratasys J750, Stratasys, Eden Prairie, MN), suggesting a possible printer-related cause for the closed vessels. The MMA models fabricated using SLA show three completely free and three completely closed models. There are also five models with partially open cavities, three of which were produced on the same 3D printer (Form 3, Formlabs Inc.). The SLA and PJ manufactured models are all liquid-tight. The partially closed cavities in SLA-manufactured models may be caused by resin residues that were not washed out. The complex design of the MMA model leads to difficulties in the orientation of the outlets on the build platform during SLA printing. In this case, the outlets should be perpendicular to the print platform to ensure good run-off of the resin residue. In addition, the comparison of blocks to MMA models shows that less complex structures are easier to print in small dimensions. Furthermore, the smaller overall length and size of the component could lead to more open cavities. In Fig. 7, the black arrows indicate the passage of the maxillary artery in the model, which was partially or completely blocked in all models. It does not seem to be possible to remove resin residues or support material entirely from an outlet without an opening.

Roughness. In a further investigation, the roughness of the materials used was analyzed using the MarSurf UD 120 roughness and contour measuring machine (Mahr GmbH, Göttingen, Germany). For this purpose, three roughness measurements (tolerance 0.1 μm) were carried out on the block at different positions, each with a scanning distance of 9.97 mm. The examination was carried out transverse to the layer direction. The roughness is evaluated using the parameters R_a (arithmetic mean roughness), R_z (mean roughness depth) and R_max (maximum roughness depth). The results are summarized in Table 2. The FDM blocks and the PJ5-8 blocks exhibit the highest roughness values of all the measured materials. The block models PJ1-4 and SLA1,2,5-8 have

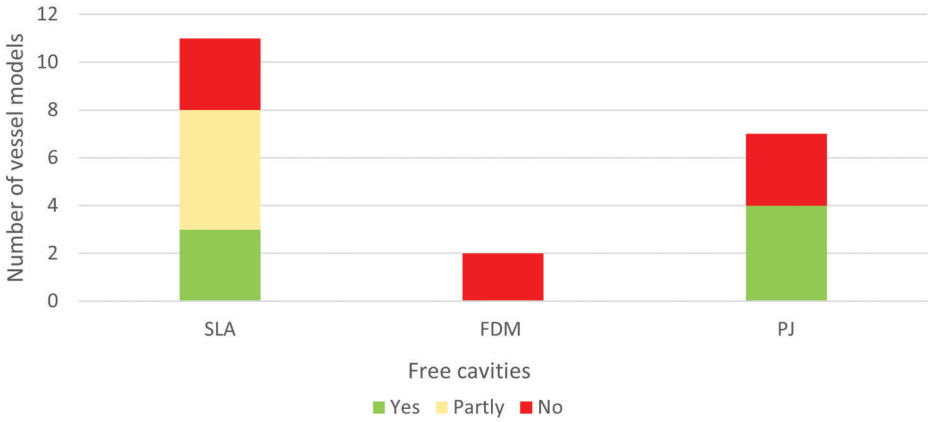

Fig. 8 Results of the cavity analysis of the different printing processes, with free cavities labeled yes (green), partially (yellow), and no (red)

comparable roughness properties, while the remaining SLA materials have the lowest roughness. The materials PJ2 and PJ3 show clearly different R_max measurements despite similar R_a values. This could indicate different surface structures despite similar average roughness. The R_max parameter can indicate extreme irregularities on the surface. A comparison of the measured roughness values with the roughness evaluations of catheter navigation by physicians can be found in the "MMA Model Application Test' section."

Water Compatibility. The water compatibility of the individual materials was analyzed in a 24-h test. First, the blocks were measured before the test using a micrometer (width and height; tolerance 0.01 mm) and a slide gauge (thickness; tolerance 0.02 mm). The blocks were subsequently placed separately from each other in circulating water at 37 °C to simulate continuous use in a fluid system. Materials that swell too much (increase >5%) or show cracks or brittleness after the test should not be considered for further study applications. These materials would not be suitable for repeated use in the simulator over several hours. After the test, the dimensions of the blocks were immediately recorded using the measuring devices mentioned above. An overview of the results of the percentage increase in the dimensions (width, height, thickness) of the blocks for the various materials after the 24-h test can be seen in Table 3. It can be Most of the materials showed a slight increase in dimensions, with only SLA8 having minimal shrinkage. No abnormal features such as brittleness or cracks could be detected in an optical inspection. The results appear to be geometry-dependent, as the greatest change in most cases concerns the thickness of the blocks. This does not exclude other influencing factors such as the manufacturing (printing direction) or the measuring method. Further investigations need to be carried out regarding these aspects, especially if material pairings are to be used for connectors in the HANNES simulator. The change in size can cause the fit to be modified and result in leaks. Further investigations are not part of this work and should be analyzed again in more detail when the material is selected.

Middle Meningeal Artery Model Application Test. To evaluate the remaining MMA models after the preliminary studies, the models were tested by physicians. For this purpose, the models were connected to the carotid artery in the HANNES simulator using the edge-free connectors. In order to achieve the same alignment of the MMA for both, hard and elastic materials, a holder was 3D printed. The models were tested with original treatment instruments in a realistic angiography suite to simulate real procedural conditions.

Table 2 Results of the roughness for the different blocks, noting the values R_a, R_z and R_max. The examination was carried out transverse to the printing direction.

Model ID	R_a (μm)	R_z (μm)	R_max (μm)
FDM1*	18.7	97.2	116.2
FDM2*	9.9	45.3	49.4
PJ1	2.4	16.2	24.5
PJ2	1.2	11.2	18.6
PJ3	1.3	8.3	10.2
PJ4	3.3	21.9	29.2
PJ5	9.2	54.7	71.0
PJ6	8.7	53.6	63.8
PJ7	11.7	65.5	79.2
PJ8*	12.1	68.8	83.8
SLA1	2.5	15.9	21.1
SLA2	1.2	5.7	6.6
SLA3	0.8	4.7	5.5
SLA4	0.1	0.3	0.4
SLA5	4.8	29.5	34.0
SLA6*	1.6	14.8	23.8
SLA7*	2.4	16.0	24.4
SLA8*	1.6	11.2	13.5
SLA9*	0.9	6.9	13.5
SLA10*	0.7	7.1	11.6

Note: The models marked with * are in-house fabrication.

Table 3 Results of the percentage increase in the dimensions (width, height, thickness) of the blocks for the different materials

Model ID	Width (mm)	Height (mm)	Thickness (mm)
FDM1*	+0.12	+0.14	+0.1
FDM2*	+0.02	+0.16	+0.0
PJ1	+0.26	+0.36	+0.1
PJ2	+0.89	+0.17	+0.1
PJ3	+0.16	+0.12	+0.2
PJ4	+0.28	+0.10	+0.1
PJ5	+0.67	+0.41	+0.1
PJ6	+0.10	+0.05	+0.1
PJ7	+0.47	+0.18	+0.2
PJ8*	−0.16	+0.15	+0.1
SLA1	+0.15	+0.06	+0.1
SLA2	+0.13	+0.14	+0.1
SLA3	+0.33	+0.45	+0.1
SLA4	+0.17	+0.05	+0.0
SLA5	+0.10	+0.15	+0.1
SLA6*	+0.22	+0.13	+0.1
SLA7*	+0.64	+0.26	+0.2
SLA8*	−0.24	−0.23	−0.1
SLA9*	+0.54	+0.47	+0.1
SLA10*	+1.45	+0.76	+0.0

Note: The models marked with * are in-house fabrication.

Two physicians with 6 and 10 years of experience in interventional neuroradiology simulated an SDH treatment to examine the MMA model in HANNES. A standard Headway^{TM} 17 microcatheter (Terumo Neuro, Shibuya, Tokyo Prefecture, Japan) was used for the study. This was inserted transfemoral into the Hannes vascular tree using a sheath and guiding catheter throughout the test. The catheter was then navigated under X-ray guidance through the existing vascular tree into the MMA. To test another MMA model, the catheter was removed to the cervical artery and then navigated from there back into the MMA model. The catheterization and flow of the MMA model were analyzed using DSA. This was done by injecting a contrast agent into the simulation model. The MMA models and their suitability for treatment simulation were initially tested without embolization. In a separate test, embolization was tested on an MMA model (see *Embolization Module Application Test*). The parameters for the evaluation of the models relate to the geometric mapping, elasticity, haptics, flow, and probing ability:

- How realistic would you rate the geometric representation of the MMA model compared to a real MMA?
- How similar would you rate the elasticity of the MMA model compared to real blood vessels during probing with the catheter?
- How similar would you rate the haptics of the MMA model compared to the existing vessel models in HANNES?
- How would you rate the internal surface smoothness of the MMA model compared to real vessels?
- Does the model show parts without flow?
- How do you rate the flow of the model?
- Was it possible to probe the model with the catheter without any problems?

The testing of the MMA was carried out by the two physicians without seeing or touching the models beforehand to prevent falsification of the results. After testing each individual model, a questionnaire was filled out to rate the evaluation criteria on a Likert scale with a score from 1 (very poor) to 5 (very good).

Geometric Mapping. The geometric mapping, which describes the real anatomical representation of the patient MMA used in the model, shows almost no differences between the individual models. The score for all MMA models was between 3 and 4 points. The more elastic materials (PJ5, PJ6, SLA5-7) were mainly rated with the lower score of 3. This might be due to the higher flexibility of the models, making them prone to shifting their positions.

Elasticity. For elasticity, the questionnaire focused on the similarity of the elasticity of the MMA models compared to real blood vessels. Points from 3 to 5 were given to the models. It would appear the physicians could not feel any great difference between elastic and hard materials, as some elastic (SLA7, PJ6) and hard (SLA8) were rated with the highest score of 5. In order to be able to make a more precise statement, this investigation should be carried out again in a large-scale study with more physicians.

Haptics. Haptic feedback is an important parameter in simulation models to imitate realistic instrument guidance as in the human body. In this test, the different MMA models were analyzed by the physicians for their similar haptic feedback to the existing vascular models in HANNES. The associated friction was also analyzed. For this purpose, the physicians were asked to compare and evaluate the MMA models with real vessel walls. All but three models were given a score of 4 and were therefore considered to have good haptic feedback and suitable friction. The SLA5 model received a moderate score of 3, while the models PJ6 and PJ8 scored less with 2 points. These models have weak haptic feedback and high friction, which is also clearly shown in the roughness measurement results (see Table 2).

Flow. To verify the flow through the model, contrast agent was injected, a DSA image series was generated and checked to ensure that all four outlets had flow. This identified clear differences between the models. The PJ5 model has a very good flowrate and was given a score of 5. The MMA model SLA1 is another well-rated model in terms of flowrate, with only the fourth outlet not being flushed (see Fig. 9(*a*)). Models SLA3 and SLA4 are rated as moderate. All other models have an insufficient to bad flow (score 1-2). A bad flowed MMA model (SLA6) with a score of 1 is shown in Fig. 9(*b*). Only half of the MMA is flushed and just 2 outlets are open.

Microcatheter Probing Ability. The DSA image series generated for the flow analysis was used to evaluate the microcatheter probing capability. The catheter was navigated through the model using the DSA image. The probing ability of the PJ5 model was rated as very good and is therefore similar to the evaluation of the flowrate. Good navigation of the catheter was observed for models SLA1, SLA3, SLA4. The catheterization of model SLA1 is shown in Fig. 9(*c*). In the MMA model SLA2, the catheter could be navigated moderately. All other models have insufficient to bad catheterization. Figure 9(*d*) shows the catheterization of the MMA model SLA6, which is rated as poor. In the PJ6 and PJ8 models, the catheter could not be navigated deep into the model due to very high wall friction perceived by the physicians. This shows a correlation with the roughness measured in the preliminary examinations, which was highest for these materials.

Summary Middle Meningeal Artery Models. Figure 10 summarizes the MMA testing and shows the exclusion of individual models after certain test steps. The FDM-manufactured MMA models already caused problems during production. The accuracy of detail is not suitable for the application of small, complex components. Furthermore, the models would have to be smoothed in a postprocessing step as they are not watertight. After the cavity and flow tests on HANNES, some SLA and PJ models were excluded.

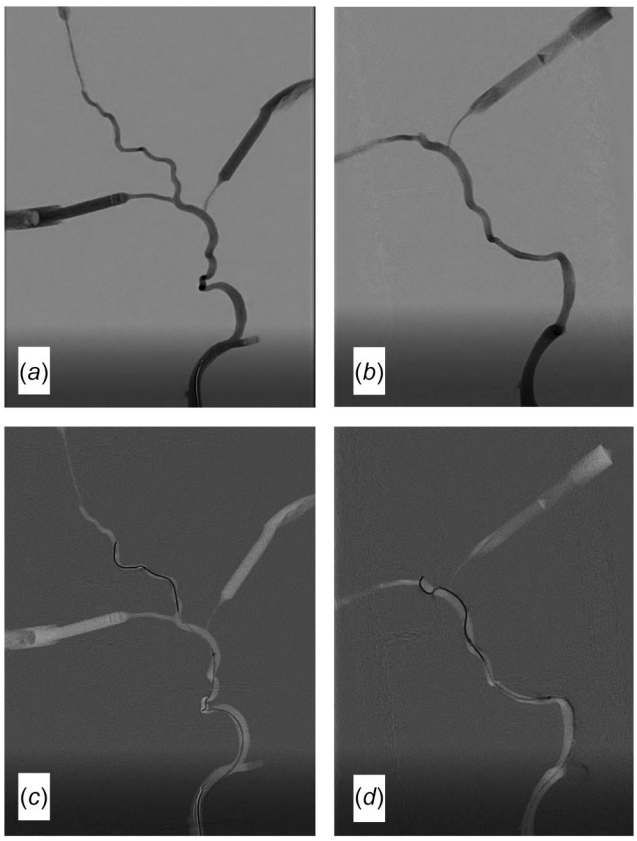

Fig. 9 DSA results of the application test with (*a*) well-flowed model SLA1, (*b*) insufficiently flowed model SLA6, (*c*) catheterization of model SLA1, highlighted by a white arrow, and (*d*) catheterization of model SLA6, highlighted by a white arrow

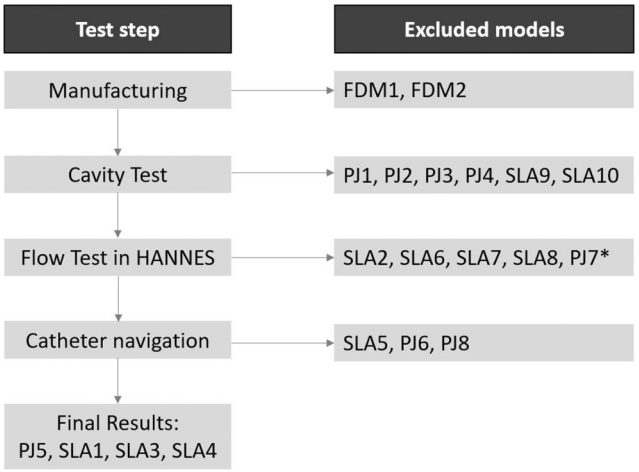

Fig. 10 Summary of the MMA tests and the exclusion of individual models after certain test steps

Resin or support residuals could be the reason for the poor cavity of the models. To improve this, the postprocessing procedures for small hollow structures should be optimized. The testing of catheter navigation showed that despite good flow, PJ materials in particular exhibit a high degree of roughness and made it impossible for the physicians to navigate the catheter. This could be improved by coating the inner surface. For all hard MMA models, a thicker wall thickness is recommended for more stability, as some outlet of the SLA1 model broke when removing outflow hoses. The remaining models after testing as well as their weighted score according to the criteria of flow, probing ability, geometric mapping, haptics, and elasticity are summarized in Table 4. The remaining four MMA models have no difference in the overall weighted evaluation with a score of 4. All models can be used for training in the simulator.

Embolization Module Preliminary Investigation. During the preliminary investigations, the behavior of the embolic agents in water and the vessel models was to be analyzed and the suitability of the module investigated. For this purpose, the module was connected to the water circuit of HANNES, but due to unknown properties of the embolic agents, it was not returned to the tank but circulated in an open system using a collecting basin. The flow sensor FCH-m-POM (B.I.O.-Tech GmbH, Vilshofen, Germany; tolerance: ±2%) integrated into HANNES was used to investigate the flowrate and was connected directly downstream of the embolization module. First, the flowrate through the membrane models with a diameter of 25 mm and the liquid-tightness were analyzed. This showed clear differences between the membrane with a pore size of 40 μm and 160 μm. With the smaller pore size, no real flow was detectable, whereas after replacing the membrane with the larger pore size, a high flow was noticeable. The models were liquid-tight in both tests. The membrane model with a diameter of 10 mm also showed a good flowrate with a pore size of 160 μm. An access to the open system was established using a sheath and catheter system inserted into the embolization module. The embolic agents, with a particle size of 45 μm to 150 μm, were mixed with water and red food coloring to make them visible, as the examination was X-ray-free. The particle embolic agent was injected into the system in small pulsed doses of 0.5 ml using a syringe to avoid blocking the catheter. A reduction in water flow was observed even after small amounts of embolic agent and complete occlusion of the module was observed after continuous embolization. Following the preliminary examination, the membrane and the corpus were washed out and connected to the previously described water circuit again to examine the flowrate. No apparent change in the flowrate compared to the first test run was observed, implying the reusability of the module.

Table 4 Summary of the models remaining after the test and their weighted evaluation

		Model ID			
Evaluation parameters	Factor	PJ5	SLA1	SLA3	SLA4
Flow	0.2	5	4	3	3
Probing ability	0.3	5	4	4	4
Geometric mapping	0.1	3	4	4	4
Haptics	0.3	4	4	4	4
Elasticity	0.1	4	3	4	3
Total score		4	4	4	4

Embolization Module Application Test. For the application test of the embolization module, one of the best-rated models from the MMA application test was adapted with an adapter for connecting the module. The SLA1 model was selected primarily due to its rapid availability. In order to test the embolization module, it was again evaluated by a physician as in the MMA application tests. For this purpose, the module was connected to the MMA artery in the HANNES simulator using the adapted adapter. The module was tested with original treatment instruments in a realistic angiography suite to simulate real procedural conditions. A standard Headway^{TM} 17 microcatheter (Terumo Neuro, Shibuya, Tokyo Prefecture, Japan) was used as in the MMA application test. This was also only inserted once into the simulator via a transfemoral sheath. To replace the models to be analyzed, the catheter was removed into the cervical artery and the next investigation was started from there. The microcatheter was navigated through the existing vascular tree and MMA up to the embolization module under X-ray guidance. The catheter position and the flow through the embolization module were detected using DSA. The test was carried out with the two membrane models described above with the same pore size of 160 μm and the different membrane diameters of 10 mm and 25 mm. The embolic particles were dissolved in contrast medium to make them radiopaque and therefore visible in the DSA. The parameters for the evaluation of the models include the realistic embolic agent distribution, flow stop by embolization, visualization, and injected amount of embolic agent. After testing each individual model, a questionnaire was filled out to rate the individual criteria with a score from 1 (very poor) to 5 (very good) or a yes/no answer.

25 mm Membrane Model. The 25 mm membrane model was tested with Contour^{TM} particles with a size of 45 μm up to 150 μm, as this size is usual for MMAE in humans. The model showed good flow without leakage (see Fig. 11(*a*)). During embolization, it could be seen under the DSA that the embolic agent was distributed over the entire membrane surface in spite of the small inflow diameter of 2 mm. After injection of the embolic agent, the flow within the model was observed to be reduced, but no complete occlusion took place (see Fig. 11(*b*)). The occlusion from the preliminary tests could not be repeated using small particles. As the model only showed a partial flow stop, this is considered insufficient for realistic treatment simulation of SDH. The next step was to use the embolic agent with larger particles (150 μm–250 μm). Here, a complete stop of the flow was detected after a typical dose of injected embolic agent in the DSA (see Fig. 11(*c*)). The embolization distribution in the module was evaluated as moderate realistic with three points. The visualization of the embolization in the module showed no complications.

10 mm Membrane Model. To compare the realistic distribution of the embolic agents, the module with the smaller membrane diameter of 10 mm was tested with the findings from the previous study with particles of 150 μm–250 μm size. The test sequence was carried out under the same conditions as the larger membrane model and the module also showed a good flowrate but leakage (see Fig. 12(*a*)). Despite that, complete occlusion could be achieved after injection of a standard therapeutic dose of the embolic agent as shown in Fig. 12(*b*). Visualization was also performed without complications in this

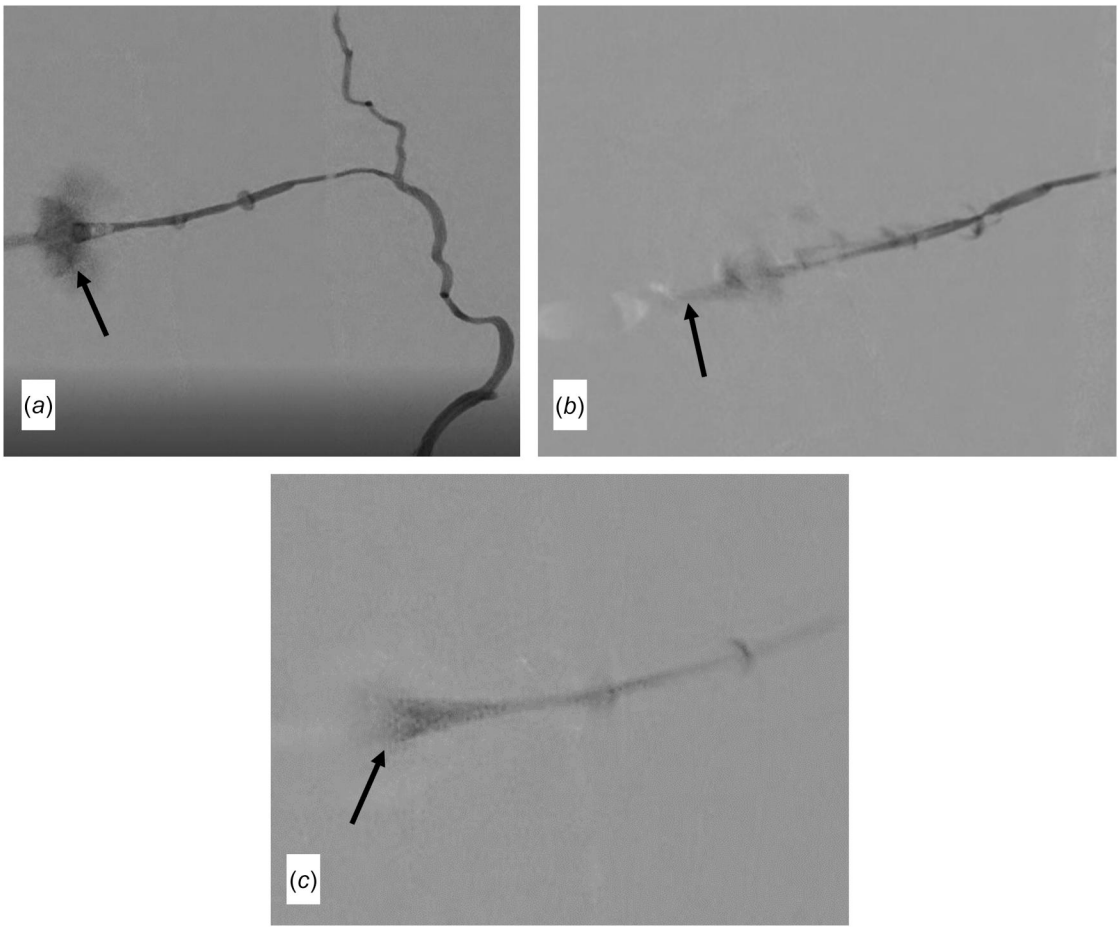

Fig. 11 Digital subtraction angiography results of the application test of the 25 mm embolization module with (*a*) flow of the contrast agent through the module (black arrow), (*b*) reduced contrast agent flow through the module (black arrow), and (*c*) complete flow stop in the module (black arrow)

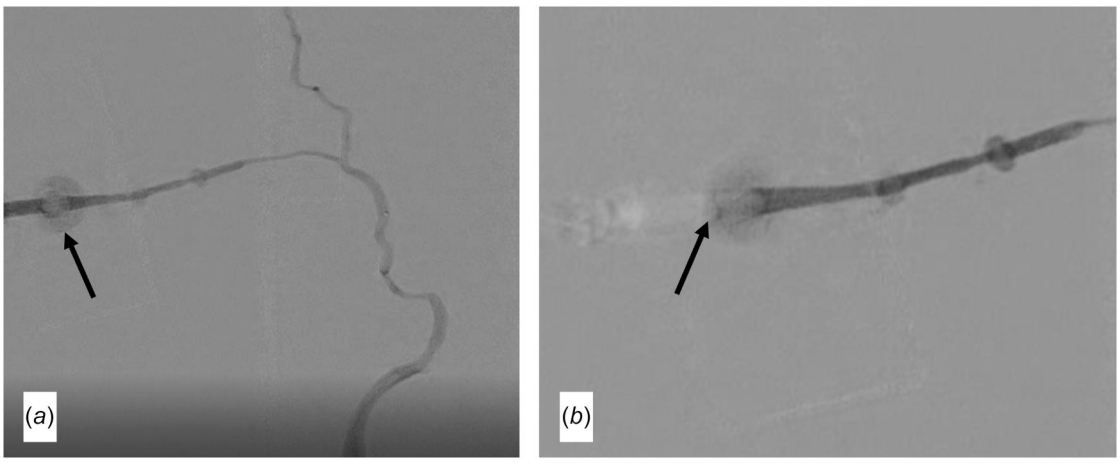

Fig. 12 Digital subtraction angiography results of the application test of the 10 mm embolization module with (*a*) flow of the contrast agent through the module (black arrow) and (*b*) complete flow stop in the module (black arrow)

procedure. The embolization distribution was rated as insufficiently realistic (score 2) and is therefore less suitable for a realistic training simulation compared to the larger membrane model.

Current Limitations

The first developed MMA model with embolization module has some limitations that will be revised as part of the optimization process. The same microcatheter was used for the application test of the 20 MMA models by the three physicians. A new one was not used for each model because of the high cost. Minimal changes in device performance are expected due to wear and tear. The model allows training in the use of the relevant treatment instruments and materials in a realistic angiography suite. To obtain a more realistic embolization distribution, the model should depict a branched vascular structure leading to the membrane and not just a single vascular branch. Furthermore, the use of other embolic agents such as liquid embolic agents should be tested covering different possible

treatments of SDH by embolization. However, due to the use of water as a blood substitute in HANNES, the model does not allow for real embolization behavior, so no body reactions on the particles, such as coagulation function, can be represented.

Conclusion

In this study, a model was developed and integrated into the existing HANNES simulator to simulate treating the small vessel disease (<2 mm) of the subdural hematoma. They rated 4 out of 20 models as sufficiently good. Relevant criteria included flowrate, probing ability, elasticity, haptics, and geometric mapping. Based on these findings, an embolization module was developed to capture particles during training, which was evaluated as a moderate baseline model for SDH embolization training. The developed MMA model with embolization module enables a first approach for the simulation of the neurointerventional procedures of SDH treatment in the HANNES simulation model with the aim of training physicians in the use of the relevant treatment instruments and materials in a realistic angiography suite and thereby improving patient safety. During the MMA model studies, problems had already arisen with the production of the two FDM models, which were not detailed enough for small, complex components and were not watertight, requiring postprocessing. Cavity and flow testing at HANNES excluded six SLA and five PJ models, possibly due to resin or support residue affecting the cavity. Catheter navigation showed that two of the PJ materials had a high surface roughness despite good flow properties, which made navigation difficult; a coating could help here. In addition, some outlets of the SLA1 models broke, indicating that the wall thickness was too low. The membrane models for embolization with Contour particle embolic agent (150 μm–250 μm) were evaluated as basic models for routinely training SDH treatment. The results showed that the membrane model with a large membrane with a diameter of 25 mm produced a more realistic representation of the embolization distribution than the small model with a membrane diameter of 10 mm. In addition, the production and postprocessing of the large models is considerably easier as evidenced by the leaks in the small membrane model. The good rated MMA models can be used in combination with a membrane model as a basic model for embolization training of SDH, but still require further revision in some cases. For a more detailed evaluation of the models, the application test should be repeated in a large-scale study with several physicians to simulate SDH treatment.

Acknowledgment

The funders had no role in study design, data collection and analysis, decision to publish, or preparation of the paper.

Funding Data

- MONTYPIE—Model for Neurointerventional Treatment in Tiny and Peripheral Vessels (Grant No. 03 LW0301K BMBF; Funder ID: 10.13039/501100002347).

Data Availability Statement

The datasets generated and supporting the findings of this article are obtainable from the corresponding author upon reasonable request.

Nomenclature

H = height
HANNES = Hamburg ANatomical NEurointerventional Simulator
R_a = arithmetic mean roughness
R_z = mean roughness depth
R_max = maximum roughness depth
T = thickness
W = width

References

[1] Schregel, K., Behme, D., Tsogkas, I., Knauth, M., Maier, I., Karch, A., Mikolajczyk, R., et al., 2018, "Optimized Management of Endovascular Treatment for Acute Ischemic Stroke," J. Visualized Exp: JoVE, (131), p. 56397.
[2] Liu, A. Y., 2006, "Update on Interventional Neuroradiology," Perm. J., **10**(1), pp. 42–46.
[3] Hacke, W., 2016, *Neurologie*, 14th ed., Springer, Berlin, Heidelberg.
[4] Saver, J. L., Chapot, R., Agid, R., Hassan, A. E., Jadhav, A. P., Liebeskind, D. S., Lobotesis, K., et al., 2020, "Thrombectomy for Distal, Medium Vessel Occlusions: A Consensus Statement on Present Knowledge and Promising Directions," Stroke, **51**(9), pp. 2872–2884.
[5] Haldrup, M., Ketharanathan, B., Debrabant, B., Schwartz, O. S., Mikkelsen, R., Fugleholm, K., Poulsen, F. R., Jensen, T. S. R., Thaarup, L. V., and Bergholt, B., 2020, "Embolization of the Middle Meningeal Artery in Patients With Chronic Subdural Hematoma-a Systematic Review and Meta-Analysis," Acta Neurochir., **162**(4), pp. 777–784.
[6] Edlmann, E., Giorgi-Coll, S., Whitfield, P. C., Carpenter, K. L. H., and Hutchinson, P. J., 2017, "Pathophysiology of Chronic Subdural Haematoma: Inflammation, Angiogenesis and Implications for Pharmacotherapy," J. Neuroinflammation, **14**(1), p. 108.
[7] Nouri, A., Gondar, R., Schaller, K., and Meling, T., 2021, "Chronic Subdural Hematoma (cSDH): A Review of the Current State of the Art," Brain Spine, **1**, p. 100300.
[8] Sila, D., Casnati, F. L., Vojtková, M., Kirsch, P., Rath, S., and Charvát, F., 2023, "Middle Meningeal Artery Embolization Versus Surgery in Patients With Chronic Subdural Hematoma-No More Fence Sitting?," Neurol. Int., **15**(4), pp. 1480–1488.
[9] Qian, Z., Yang, D., Sun, F., and Sun, Z., 2017, "Risk Factors for Recurrence of Chronic Subdural Hematoma After Burr Hole Surgery: Potential Protective Role of Dexamethasone," Br. J. Neurosurg., **31**(1), pp. 84–88.
[10] Bonasia, S., Smajda, S., Ciccio, G., and Robert, T., 2020, "Middle Meningeal Artery: Anatomy and Variations," Am. J. Neuroradiol., **41**(10), pp. 1777–1785.
[11] Arturo Larco, J. L., Madhani, S. I., Liu, Y., Abbasi, M., Lylyk, P. N., Benike, A., Shahid, A., Tekin, B., Quinton, R., and Savastano, L. E., 2023, "Evaluation of an in Vivo Preclinical Model for Human Middle Meningeal Artery Embolization Using the Posterior Intercostal Artery of the Swine," J. Neurointerventional Surg., **15**(9), pp. 924–930.
[12] Mokin, M., Pionessa, D., Koenigsknecht, C., Gutierrez, L., Nagesh, S. V. S., Tuttle, K. M. M., Spengler, M., et al., 2025, "A Novel Swine Model of Selective Middle Meningeal Artery Catheterization and Embolization," J. Neurointerventional Surg., **17**(2), pp. 210–214.
[13] D'Abbondanza, J. A., and Loch Macdonald, R., 2014, "Experimental Models of Chronic Subdural Hematoma," Neurol. Res., **36**(2), pp. 176–188.
[14] Chen, H., Colasurdo, M., and Kan, P. T., 2024, "Middle Meningeal Artery Embolization as Standalone Treatment Versus Combined With Surgical Evacuation for Chronic Subdural Hematomas: Systematic Review and Meta-Analysis," J. Neurosurg., **140**(3), pp. 819–825.
[15] Liu, W., Bakker, N. A., and Groen, R. J. M., 2014, "Chronic Subdural Hematoma: A Systematic Review and Meta-Analysis of Surgical Procedures," J. Neurosurg., **121**(3), pp. 665–673.
[16] Tiwari, A., Dmytriw, A. A., Bo, R., Farkas, N., Ye, P., Gordon, D. S., Arcot, K. M., Turkel-Parrella, D., and Farkas, J., 2021, "Recurrence and Coniglobus Volumetric Resolution of Subacute and Chronic Subdural Hematoma Post-Middle Meningeal Artery Embolization," Diagnostics, **11**(2), p. 257.
[17] Xu, C.-S., Lu, M., Liu, L.-Y., Yao, M.-Y., Cheng, G.-L., Tian, X.-Y., Xiao, F., Wan, Q., and Chen, F., 2017, "Chronic Subdural Hematoma Management: Clarifying the Definitions of Outcome Measures to Better Understand Treatment Efficacy - A Systematic Review and Meta-Analysis," Eur. Rev. Med. Pharmacol. Sci., **21**(4), pp. 809–818.
[18] Abdollahifard, S., Farrokhi, A., Yousefi, O., Valibeygi, A., Azami, P., and Mowla, A., 2024, "Particle Embolic Agents for Embolization of Middle Meningeal Artery in the Treatment of Chronic Subdural Hematoma: A Systematic Review and Meta-Analysis," Interventional Neuroradiol., **30**(1), pp. 94–104.
[19] Ban, S. P., Hwang, G., Byoun, H. S., Kim, T., Lee, S. U., Bang, J. S., Han, J. H., Kim, C.-Y., Kwon, O.-K., and Oh, C. W., 2018, "Middle Meningeal Artery Embolization for Chronic Subdural Hematoma," Radiology, **286**(3), pp. 992–999.
[20] Omura, Y., and Ishiguro, T., 2023, "Middle Meningeal Artery Embolization for Chronic Subdural Hematoma: A Systematic Review," Front. Neurol., **14**, p. 1259647.
[21] Hai, D. X., Thong, P. M., He, D.-V., Le Dung, T., Hung, D. D., Huyen, N.-T., and Minh Duc, N., 2024, "Outcomes of Middle Meningeal Artery Embolization for Treating Chronic Subdural Hematoma," Ital. J. Med., **18**(3), p. 1759.
[22] Fiehler, J., and Bechstein, M., 2024, "Does Every Subdural Hematoma Patient Need an Embolization?," Clin. Neuroradiol., **34**(2), pp. 289–291.
[23] Sadasivan, C., Dashti, N., Marfoglio, S., and Fiorella, D., 2024, "In Vitro Comparison of Middle Meningeal Artery Embolization With Squid Liquid Embolic Agent and Contour Polyvinyl Alcohol Particles," J. Neurointerventional Surg., **16**(3), pp. 280–284.
[24] Ku, J. C., Dmytriw, A. A., Essibayi, M. A., Banihashemi, M. A., Vranic, J. E., Ghozy, S., Altschul, D., et al., 2023, "Embolic Agent Choice in Middle Meningeal Artery Embolization as Primary or Adjunct Treatment for Chronic Subdural Hematoma: A Systematic Review and Meta-Analysis," Am. J. Neuroradiol., **44**(3), pp. 297–302.
[25] Sioutas, G. S., Vivanco-Suarez, J., Shekhtman, O., Matache, I.-M., Salem, M. M., Burkhardt, J.-K., Srinivasan, V. M., and Jankowitz, B. T., 2023, "Liquid Embolic Agents for Middle Meningeal Artery Embolization in Chronic Subdural Hematoma: Institutional Experience With Systematic Review and Meta-Analysis," Interventional Neuroradiol., p. 15910199231183132.

[26] Shehabeldin, M., Amllay, A., Jabre, R., Chen, C.-J., Schunemann, V., Herial, N. A., Gooch, M. R., et al., 2023, "Onyx Versus Particles for Middle Meningeal Artery Embolization in Chronic Subdural Hematoma," Neurosurgery, **92**(5), pp. 979–985.
[27] Ellens, N. R., Schartz, D., Kohli, G., Rahmani, R., Akkipeddi, S. M. K., Mattingly, T. K., Bhalla, T., and Bender, M. T., 2024, "Safety and Efficacy Comparison of Embolic Agents for Middle Meningeal Artery Embolization for Chronic Subdural Hematoma," J. Cerebrovasc. Endovasc. Neurosurg., **26**(1), pp. 11–22.
[28] Tudor, T., Capone, S., Vivanco-Suarez, J., Salem, M. M., Sioutas, G. S., Tonetti, D. A., Heiferman, D. M., et al., 2024, "Middle Meningeal Artery Embolization for Chronic Subdural Hematoma: A Review of Established and Emerging Embolic Agents," Stroke: Vasc. Interventional Neurol., **4**(1), p. e000906.
[29] Nawka, M. T., Fiehler, J., Spallek, J., Buhk, J.-H., and Frölich, A. M., 2019, "Current Status of Training Environments in Neuro-Interventional Practice: Are Animal Models Still Contemporary?," J. Neurointerventional Surg., **11**(3), pp. 283–289.
[30] Tian, Y., Wang, D., Zhang, X., Wei, H., Wei, Y., An, S., Gao, C., et al., 2022, "Establishment and Validation of a Prediction Model for Self-Absorption Probability of Chronic Subdural Hematoma," Front. Neurol., **13**, p. 913495.
[31] Ni, Z., Zhu, Y., Qian, Y., Li, X., Xing, Z., Zhou, Y., Chen, Y., Huang, L., Yang, J., and Zhuge, Q., 2024, "Synthetic Minority Over-Sampling Technique-Enhanced Machine Learning Models for Predicting Recurrence of Postoperative Chronic Subdural Hematoma," Front. Neurol., **15**, p. 1305543.
[32] Post, A., Hoshizaki, T. B., Gilchrist, M., and Brien, S., 2012, "Analysis of the Influence of Independent Variables Used for Reconstruction of a Traumatic Brain Injury Incident," Proc. Inst. Mech. Eng., Part P, **226**(3–4), pp. 290–298.
[33] Deck, C., and Willinger, R., 2008, "Improved Head Injury Criteria Based on Head FE Model," Int. J. Crashworthiness, **13**(6), pp. 667–678.
[34] Sarkar, S., Roychowdhury, A., and Ghosh, U., 2008, "Prediction of Subdural Haematoma Based on a 3D Finite Element Human Head Model," Int. J. Veh. Saf., **3**(3), p. 276.
[35] Abdollahifard, S., Farrokhi, A., and Mowla, A., 2023, "Application of Deep Learning Models for Detection of Subdural Hematoma: A Systematic Review and Meta-Analysis," J. Neurointerventional Surg., **15**(10), pp. 995–1000.
[36] Inomata, T., Nakaya, K., Matsuhiro, M., Takei, J., Shiozaki, H., and Noda, Y., 2024, "Clinical Use of Hematoma Volume Based On Automated Segmentation of Chronic Subdural Hematoma Using 3D U-Net," Clin. Neuroradiol., **34**(4), pp. 799–807.
[37] Candefjord, S., Winges, J., Malik, A. A., Yu, Y., Rylander, T., McKelvey, T., Fhager, A., Elam, M., and Persson, M., 2017, "Microwave Technology for Detecting Traumatic Intracranial Bleedings: Tests on Phantom of Subdural Hematoma and Numerical Simulations," Med. Biol. Eng. Comput., **55**(8), pp. 1177–1188.
[38] Spallek, J., Kuhl, J., Wortmann, N., Buhk, J.-H., Frölich, A. M., Nawka, M. T., Kyselyova, A., Fiehler, J., and Krause, D., 2019, "Design for Mass Adaptation of the Neurointerventional Training Model HANNES With Patient-Specific Aneurysm Models," Proc. Int. Conf. Eng. Des., **1**(1), pp. 897–906.
[39] Wortmann, N., Spallek, J., Kyselyova, A. A., Frölich, A. M., Fiehler, J., and Krause, D., 2019, "Concept of an In-Vitro Model for Endovascular Stroke Treatment Using Additive Manufacturing," Trans. Addit. Manuf. Meets Med., **1**(1), Article No. S04T03.
[40] Spallek, J., Wortmann, N., Kuhl, J., Wegner, M., and Krause, D., 2020, "Entwicklung Und Anwendung Medizinischer Simulationsmodelle," *Produktentwicklung Und Konstruktionstechnik: Forschungsergebnisse Und -Projekte Der Jahre 2016 bis 2020*, Krause D., Hartwich T. S., and Rennpferdt C., eds., Springer Vieweg, Berlin, Heidelberg, pp. 255–272.
[41] Schmiech, J., Wegner, M., Wortmann, N., Sobirey, E., Guerreiro, H., Kyselyova, A., Ramdani, N., and Krause, D., 2025, "HANNES: A Modular Neurointerventional Training Model," ASME J. Eng. Sci. Med. Diagn. Ther., **8**(3), p. 031008.
[42] Vdi Verein Deutscher Ingenieure e, V., 2019, *Hrsg.:, VDI 2221 Blatt 1 - Entwicklung Technischer Produkte Und Systeme - Modell Der Produktentwicklung*, Beuth-Verlag, Berlin, Germany.
[43] Wegner, M., Schmiech, J., Sobirey, E., Krause, D., and Gargioni, E., 2024, "Requirement Analysis in Medical Phantom Development: A Survey Tool Approach With an Illustrative Example of a Multimodal Deformable Pelvic Phantom," Front. Phys., **12**, p. 1416601.